AIP | Applied Physics Letters

Hot spot engineering for light absorption enhancement of solar cells with a super-structured transparent conducting electrode

R. Smaali, E. Centeno, and A. Moreau

Citation: Appl. Phys. Lett. **103**, 113905 (2013); doi: 10.1063/1.4821156
View online: http://dx.doi.org/10.1063/1.4821156
View Table of Contents: http://apl.aip.org/resource/1/APPLAB/v103/i11
Published by the AIP Publishing LLC.

Hot spot engineering for light absorption enhancement of solar cells with a super-structured transparent conducting electrode

R. Smaali,[1,2] E. Centeno,[1,2] and A. Moreau[1,2]
[1]*Institut Pascal, Clermont Université, Université Blaise Pascal, BP 10448, F-63000 Clermont-Ferrand, France*
[2]*CNRS, UMR 6602, Institut Pascal, F-63177 Aubière, France*

(Received 19 April 2013; accepted 11 August 2013; published online 13 September 2013)

We study the impact of a super-structuration of the transparent conducting electrode made of polycrystalline ZnO:Al on the efficiency of thin solar cells based on amorphous silicon. We demonstrate that photonic crystal cavities etched in the electrode present efficient anti-reflective properties and add absorption resonances in the red part of the spectrum where other structures are inefficient. This super-structuring boosts the optical absorption by 4.2% and broaden the angular acceptance compared to conventional grating patterns. The origin of these cavity states is explained in the framework of the envelop function approach. © *2013 AIP Publishing LLC*. [http://dx.doi.org/10.1063/1.4821156]

Trapping light in very thin amorphous silicon layers is a timely issue for realizing efficient and low cost second generation photovoltaic cells. It is, in particular, challenging in the red part of the solar spectrum where the absorbance of amorphous silicon is very weak, and its thickness can be three or four times smaller than the wavelength. In this context, different approaches stemming on the nano-patterning of the silicon layer,[1–3] the anti-reflective coating,[4–7] or the electrodes[8] aim at increasing the light path within the active layer. Enhanced absorption has been observed in photonic crystal[9,10] or plasmonic[11,12] based devices where the periodic structuring generates resonant electromagnetic modes strongly confined within the absorber. These approaches, based on periodic structures, make it however difficult to match the set of resonant frequencies with the entire absorption range. The angular acceptance is, in addition, reduced because such resonances are associated to Bloch modes that are highly delocalized. On the other hand, the resonant frequency window can be extended by introducing a controlled disorder[13,14] in the structure. Disorder drastically changes the distribution of light along the absorber by creating localized states. By virtue of the Heisenberg principle, these highly confined states are strongly delocalized in the wavevector space, allowing a broad angular coupling with the incident solar radiations. In this work, we develop an alternative approach that generates hot spots in the spectral window where the absorption coefficient of the active layer is low, and the periodic texturing is inefficient. For that purpose, we consider a periodic patterning that integrates an appropriate defect whose resonances are tuned at the desired wavelength. Our device is, in particular, constituted of a non-textured amorphous silicon layer (a-Si:H) coated with an electrode presenting a 1D superlattice. Our previous study[8] has shown that a 1D grating drilled in the transparent electrode behaves like an anti-reflective layer and introduces resonant modes that enhance the optical absorption by 10%. This approach provides an optimal optical solution and prevents electron-hole recombinations inside the active layer. Here, we improve these results through an in-plane localization effect, leading to a 4.2% additional optical absorption with a large angular acceptance of 12°. The origin of this enhancement is explained in the framework of a perturbation theory developed for PhC heterostructures[15] that guide us for the design of optimized devices.

The proposed thin-film solar cells consists, from back to front, of a perfect electric conductor, a Al-doped zinc oxide (ZnO:Al) spacer, an unpatterned a-Si:H layer (the absorber), and a textured ZnO:Al electrode, as shown in Fig. 1. Remark that optical absorption for both ZnO:Al spacer and electrode is considered.[16–18] The optical performance of the superlattice transparent conducting electrode (SL-TCE) and grating electrode (G-TCE) are theoretically compared by keeping all the geometrical parameters fixed (thicknesses, grating period d, filling factor f). The SL-TCE consists of periodic grooves of depth h_r drilled in the ZnO:Al layer with a period d. The superlattice is obtained by removing one ZnO:Al slot at each macro-periods $D = 2Nd$. Finally, our SL-TCE can be considered as a supercell of length D that comprises an optical cavity of width $L = d$. The absorption $A(\lambda)$ in the a:Si layer is numerically computed using a rigorous couple wave method[19] and is dependent on the polarization (TE or TM) of the incoming light (for details concerning its numerical computation, see Ref. 8). Assuming an optimal internal quantum efficiency (i.e., electron-hole recombination are neglected), the short-circuit current density j_{sc} is given by the conventional definition

$$j_{sc} = \int A(\lambda) \frac{dI}{d\lambda} \frac{e\lambda}{hc} \, d\lambda, \tag{1}$$

where $\frac{dI}{d\lambda}$ is the spectral energy density given by an Am 1.5G normalized spectrum. The current density enhancement $CDE = j_{sc}/j_{max}$ is defined as the ratio of j_{sc} over the maximum short-circuit current obtained when all the incident photons of the considered spectral range (from 375 nm to 750 nm) are converted into excitons ($j_{max} = 23.665\,\mathrm{mA/cm^2}$).[20] The unpolarized nature of the solar spectrum is modeled by averaging the *CDE* over both polarizations. With these definitions, the *CDE* represents the upper bound of the current density enhancement. We start by optimizing the SL-TCE using a

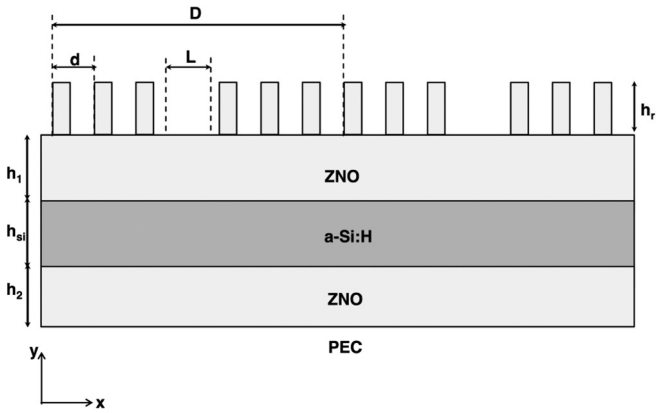

FIG. 1. Schematic diagram of a solar cell.

home-made genetic algorithm[21] and by imposing a maximal thickness for the silicon layer of 150 nm. We obtain a short circuit current $j_{sc} = 14.91\,\mathrm{mA\,cm^{-2}}$ and a $CDE = 63.01\%$ for the following geometrical parameters: $h_{si} = 147\,\mathrm{nm}$, $h_r = 379\,\mathrm{nm}$, $d = 459\,\mathrm{nm}$, $h_1 = 52\,\mathrm{nm}$, $h_2 = 237\,\mathrm{nm}$, and it is reached when 4 grating pitches separate each cavity giving a supercell of period $D = 8d$. We underline that the optimal geometrical parameters only slightly change with the number of pitches separating each cavities. The optimal filling factor, defined as the ratio between the width of ZnO:Al slot and the pitch of the grating d, is found to be $f = 0.51$. Let us now evaluate the gain on light absorption induced by such optical cavities by comparing with a 1D grating electrode. For the same geometrical parameters but without the presence of any cavity, the G-TCE yields a short circuit current $j_{sc} = 14.32\,\mathrm{mA\,cm^{-2}}$ and $CDE = 60.51\%$. This result demonstrates that the superstructuring used in the SL-TCE enhances the light absorption since the relative increase of the *CDE* reaches 4.2% compared to the G-TCE. The absorption spectra plotted in Fig. 2 shows that extra absorption lines (solid lines) appear in the range of wavelength $700 - 750\,\mathrm{nm}$ where the G-TCE is inefficient. A large resonance arises in particular at 712 nm for TM polarization and a smaller one is observed for TE polarization at 702 nm. In this spectral window ($700 - 750\,\mathrm{nm}$), the SL-TCE solar cell allows an increase of the *CDE* by a factor 3 and 7 for TE and TM polarization cases, respectively. The rest of the absorption spectrum ($375 - 700\,\mathrm{nm}$) is only slightly affected by the optical cavities and actually presents a noticeable increase too. The superlattice structure has in addition a large angular acceptance since the current density enhancement is higher than 60% until an inclination of 12° and remains larger than 55% in oblique incidence (Fig. 3). This result confirms that the hot light spots localized in the cavities can equally be addressed out of normal incidence. Moreover, for the SL-TCE, the *CDE* is almost always larger than that obtained with the G-TCE, leading to a 3% enhancement of the average current density enhancement over all incident angles. The maximal *CDE* is reached in normal incidence for the superlattice while it is observed at 7° for the grating electrode. This shift originates from the broken lattice symmetry induced by the cavity which allows an efficient coupling with the Bloch modes in normal incidence.

To explain the origin of these extra-absorption peaks, we use an envelop function approach already applied to heterostructured photonic crystals.[15] The large size of our supercell ($D = 8d$) allows us to assume a weak coupling between the optical cavities. This leads to identify our supercell (depicted in Fig. 1) to an heterostructure. The origin of the cavity resonances can be understood using a perturbative scheme: our cavity is a perturbation of the grating electrode that shifts its resonances in the appropriate wavelength window. The strength and the direction of this frequency offset depend on the nature of the defect introduced in the lattice. A clear picture of this dynamic is given by the envelop function approach where the n-th cavity mode $\mathbf{E}_{\mathbf{k}}^{(\mathbf{n})}(\mathbf{r})$ is linked to the unperturbed Bloch mode $\mathbf{E}_{\mathbf{k}}(\mathbf{r})$ lying at a band gap edge by a slowly varying function $f_{\mathbf{k}}^{(n)}(r)$: $\mathbf{E}_{\mathbf{k}}^{(\mathbf{n})}(\mathbf{r}) = \mathbf{f}_{\mathbf{k}}^{(\mathbf{n})}(\mathbf{r})\mathbf{E}_{\mathbf{k}}(\mathbf{r})$. The spatial variations of $f_{\mathbf{k}}^{(n)}(r)$ at the scale of the heterostructure are dictated by a Schrödinger-like wave equation, which in 1D reads

$$\frac{1}{2m_{eff}} \times \frac{d^2 f_{k_0}^{(n)}(x)}{dx^2} = \left[\omega_{k_0}^2 - \omega_n^2(1 + \Delta(x))\right] f_{k_0}^{(n)}(x), \qquad (2)$$

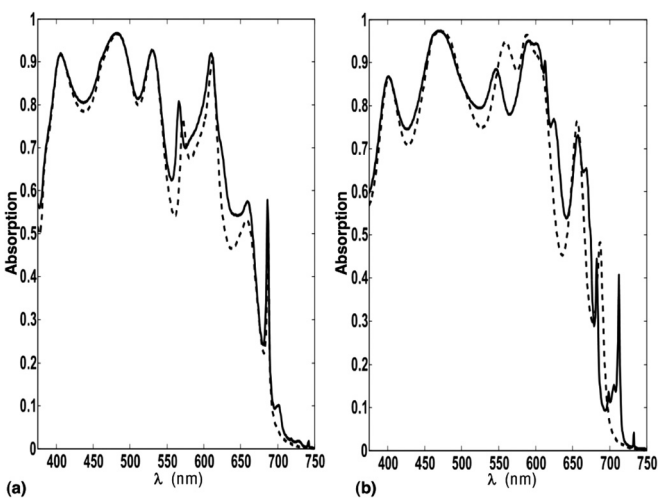

FIG. 2. TE polarization: (a) absorption of the a-Si:H layer for G-TCE (dashed line), SL-TCE (solid line). TM Polarization: (b) absorption of the a-Si:H layer for G-TCE (dashed line), SL-TCE (solid line).

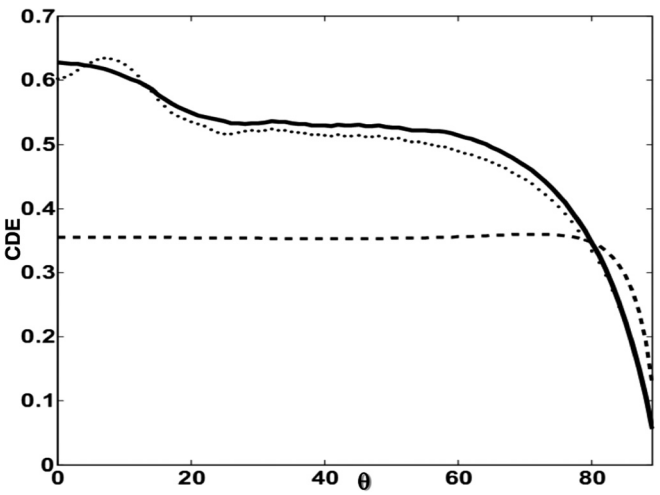

FIG. 3. The current density enhancement (averaged over both polarizations) as a function of the angle incidence θ° (TE or TM polarization are maintained whatever θ°). For a silicon layer of thickness $h_{si} = 147\,\mathrm{nm}$ coated with the SL-TCE (solid line), with the G-TCE (dot curve), and without the transparent electrode (dashed line).

where m_{eff} denotes the effective mass of the unperturbed Bloch mode at specific wavevector k_0 defined by $\frac{1}{m_{eff}} = \frac{\partial^2 \omega_n^2}{\partial k_x^2}|_{k_0}$. The frequency ω_{k_0} corresponds to the unperturbed Bloch mode and ω_n is the n-th resonant frequencies sustain by the cavity. The function $\Delta(x)$ is equivalent to the potential function for the equivalent quantum well problem. We look at propagating waves inside the cavity (for $|x| < L/2$), where $\Delta(x) = \Delta_0$ while outside the cavity, where $\Delta(x) = 0$, the waves are evanescent

$$f_{nk_0}(x) = \begin{cases} A\cos(Kx) + B\sin(Kx) & \text{for} \quad |x| < L/2, \\ Ce^{-\gamma x} & \text{for} \quad |x| > L/2. \end{cases} \tag{3}$$

The propagating constants are given by

$$K = \sqrt{2m_{eff}[\omega_{\lambda n}^2(1+\Delta_0) - \omega_n^2(k_0)]}, \tag{4}$$

$$\gamma = \sqrt{2m_{eff}(\omega_n^2(k_0) - \omega_{\lambda n}^2)}. \tag{5}$$

Practically, the perturbation Δ_0 induced by the cavity is related to the variation of the permittivity along the electrode. The effective permittivities ϵ_{Grat} and ϵ_{Cav} in the grating and cavity area are analytically obtained through a homogenization process which allows to derive $\Delta_0 = \frac{\epsilon_{Cav}}{\epsilon_{Grat}} - 1$. In our case, these effective permittivities are $\epsilon_{Grat} = 1.36$ and $\epsilon_{Cav} = 1$ inside the air-cavity leading to $\Delta_0 = -0.267$. The odd and even modes of the cavity satisfy the following transcendental equation, deduced from the continuity of the envelope function and its derivative at $x = L/2$

$$K = \gamma \tan(KL - \sigma), \tag{6}$$

where $\sigma = 0$ for even modes and $\sigma = \pi/2$ for odd modes. These equations are solved by considering the following dispersion equation:

$$K^2 + \gamma^2(1+\Delta_0) = 2m_{eff}\omega_{k_0}^2\Delta_0. \tag{7}$$

The allowed index contrast between the cavity and the grating area imposes that $1 + \Delta_0 > 0$. Equation (6) is then satisfied when the product $m_{eff}\Delta_0$ is positive. This implies that the sign of Δ_0 defines which Bloch modes are allowed to shift inside the gap. Here, only Bloch modes presenting a negative effective mass forms the resonant spectrum of the cavity since $\Delta_0 = -0.267$. To confirm this theory, we have computed the dispersion relations of the eigenmodes when the wavevector, k_x, ranges in the first Brillouin zone (Fig. 4). For that purpose, the dispersion of the optical index for silicon is neglected (the refractive index and the absorption coefficient are fixed to the corresponding value for $\lambda = 700\,\text{nm}$). For TE polarization, the grating mode corresponding to $\lambda = 706\,\text{nm}$ and $k_x = 0$ presents a negative effective mass $m_{eff} = -0.082c^{-2}$. The resolution of transcendental Eq. (5) provides a resonant wavelength of 692 nm

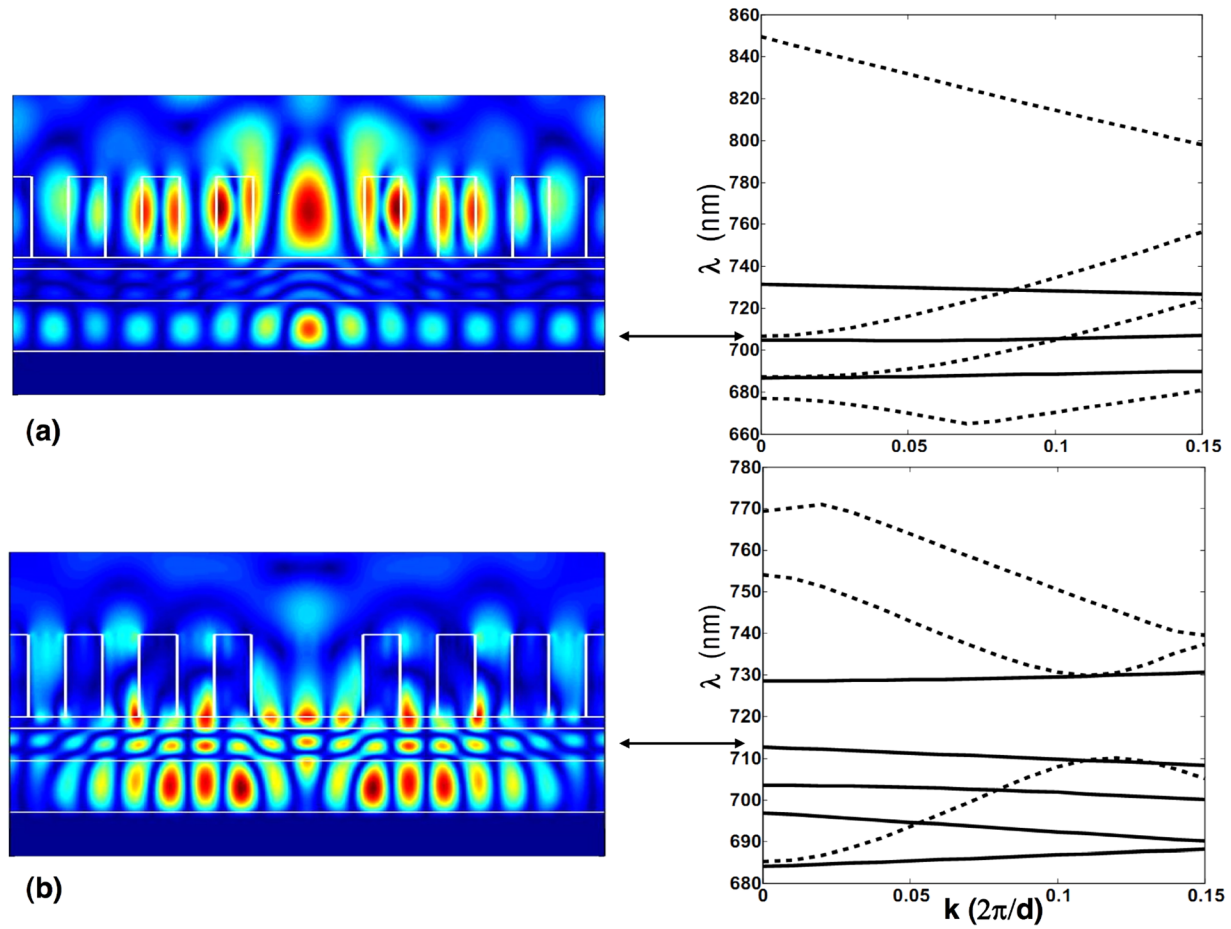

FIG. 4. TE polarization: (a) electric field @$\lambda = 702.4\,\text{nm}$ (left), diagram dispersion (right). TM polarization: (b) electric field @$\lambda = 712.5\,\text{nm}$ (left), diagram dispersion (right).

associated to the fundamental even mode of the cavity. The envelop function method predicts with an error smaller than 2% the absorption peak seen in Fig. 2(a) for $\lambda = 702$ nm. Similarly, the absorption line arising at $\lambda = 712$ nm in TM polarization is also explained by the red-shift of a grating Bloch mode. In that case, the perturbative method gives a resonant odd mode for $\lambda = 714$ nm in agreement with the exact value (Fig. 2(b)). However, this cavity mode originates from a Bloch mode of negative mass $m_{eff} = -0.63c^{-2}$ that appears at the edge of the Brillouin zone (at $k_x = \pi/d$). The difference between the efficiencies of absorption lines for the TE and TM polarization is explained by the location of the resonant modes within the depth of the solar cell. It can be seen that the TE mode is almost confined in the lower refractive index materials, i.e., in the structured electrode and the ZnO:Al spacer (Fig. 4). On the contrary, for TM polarization, the resonant state is highly confined within the silicon layer which explains the huge resonant peak observed in the absorption spectrum of Fig. 2. The other modes observed in the dispersion diagram are not confined in the cavity and correspond to negligible absorption lines. Since ZnO:Al is absorbent in the visible range of wavelengths, the parasitic absorption in the TCE is not negligible.[16] We quantify this parasitic absorption by calculating the ratio of optical absorption in ZnO:Al layers (electrode and spacer) over the absorption in the a-Si:H absorber: $\rho_p = A_{ZnO}/A_{Si}$. This parasitic absorption is higher for the TE resonant mode with $\rho_p = 1.8$ than for the TM cavity mode $\rho_p = 0.8$, according to their spatial distribution within the cell (Fig. 4). Finally, the parasitic absorption is shown to strongly depend on the light polarization. This effect is expected to be drastically reduced when considering a 2D superlattices that provide a full in-plane confinement of light and make the optical properties of the cells more isotropic.

In conclusion, a thin silicon absorbing layer coated with properly super-structured transparent conducting electrodes supports additional absorption lines in the frequency range where the sole periodic patterning is inefficient. Optical cavities periodically etched within the grating provide an in-plane localization effect that increases light absorption. The envelop function method has shown to be a reliable approach to design optical cavity presenting additional resonances in the appropriate absorption spectrum. This hot spot engineering approach suggests that superlattice has a real potential for the design of future optimized solar cells. In particular, the two-dimensional super-structuring of the transparent electrode is expected to render more isotropic, the optical efficiency of such Photovoltaics cells reducing the polarization dependence and the frequency shift in oblique incidence of the cavity modes. Thin absorbers coated with superlattice drilled into the transparent electrode is a simple and efficient approach that optimizes both the optical absorption and the electronic transport.

This work was supported by the French Laboratory of excellence IMobS3. The authors thank the Centre Informatique National de l'Enseignement Supérieur for its computing support.

[1]Y. Park, E. Drouard, O. E. Daif, X. Letartre, P. Viktorovitch, A. Fave, A. Kaminski, M. Lemiti, and C. Seassal, Opt. Express **17**, 14312 (2009).
[2]O. E. Daif, E. Drouard, G. Gomard, A. Kaminski, A. Fave, M. Lemiti, S. Ahn, S. Kim, P. R. i Cabarrocas, H. Jeon, and C. Seassal, Opt. Express **18**, A293 (2010).
[3]S. Mallick, M. Agrawal, and P. Peumans, Opt. Express **18**, 5691 (2010).
[4]S. S. Lo, C.-C. Chen, F. Garwe, and T. Pertch, J. Phys. D: Appl. Phys. **40**, 754 (2007).
[5]M. Kroll, S. Fahr, C. Helgert, C. Rockstuhl, F. Lederer, and T. Pertsch, Phys. Status Solidi A **205**, 2777 (2008).
[6]R. Dewan and D. Knipp, J. Appl. Phys. **106**, 074901 (2009).
[7]S. Zanotto, M. Liscidini, and L. C. Andreani, Opt. Express **18**, 4260 (2010).
[8]A. Moreau, R. Smaali, E. Centeno, and C. Seassal, J. Appl. Phys. **111**, 083102 (2012).
[9]R. Peretti, G. Gomard, C. Seassal, X. Letarte, and E. Drouard, J. Appl. Phys. **111**, 123114 (2012).
[10]X. Meng, G. Gomard, O. E. Daif, E. Drouard, R. Orobtchouk, A. Kaminski, A. Fave, M. Lemiti, A. Abramov, P. R. i Cabarrocas, and C. Seassal, Sol. Energy Mater. Sol. Cells **95**, S32 (2011).
[11]S. Pillai, K. R. Catchpole, T. Trupke, and M. A. Wiersma, J. Appl. Phys. **101**, 093105 (2007).
[12]K. Q. Le, A. Abass, B. Maes, P. Bienstman, and A. Alu, Opt. Express. **20**, A39 (2012).
[13]K. Vynck, M. Buressi, F. Ribolli, and D. S. Wiersma, Nature Mater. **11**, 1017 (2012).
[14]A. Oskooi, P. Favuzzi, Y. Tanak, H. Shigeta, and Y. Kawakami, Appl. Phys. Lett. **100**, 181110 (2012).
[15]M. Chabonneau-Lefort, E. Istrate, M. Allard, J. Poon, and E. Sargent, Phys. Rev. B **65**, 125318 (2002).
[16]F. Ruske, M. Wimmer, G. Koppel, A. Pflug, and B. Rech, Proc. SPIE **8263**, 826303 (2012).
[17]N. Shakti and P. S. Gupta, Appl. Phys. Res. **2**, 19 (2010).
[18]S. Ilican, Y. Caglar, and M. Caglar, J. Optoelectron. Adv. Mater. **10**, 2578 (2008).
[19]G. Granet and B. Guizal, J. Opt. Soc. Am. A **13**, 1019 (1996).
[20]W. Shockely and H. J. Queisser, J. Appl. Phys. **32**, 510 (1961).
[21]D. Goldberg, *Genetic Algorithms* (Addison Wesley, 1989).